

Cytochrome *c* Provides an Electron-Funneling Antenna for Efficient Photocurrent Generation in a Reaction Center Biophotocathode

Vincent M. Friebe,[†] Diego Millo,[†] David J. K. Swainsbury,^{‡,§} Michael R. Jones,[‡] and Raoul N. Frese^{*,†}

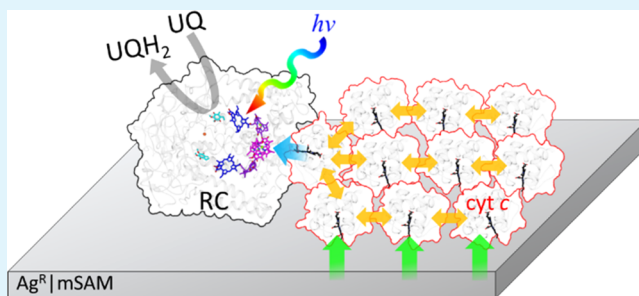
[†]Department of Physics and Astronomy, LaserLaB Amsterdam, VU University Amsterdam, De Boelelaan 1081, Amsterdam 1081 HV, The Netherlands

[‡]School of Biochemistry, University of Bristol, Medical Sciences Building, University Walk, Bristol BS8 1TD, U.K.

S Supporting Information

ABSTRACT: The high quantum efficiency of photosynthetic reaction centers (RCs) makes them attractive for bioelectronic and biophotovoltaic applications. However, much of the native RC efficiency is lost in communication between surface-bound RCs and electrode materials. The state-of-the-art biophotocathodes utilizing cytochrome *c* (cyt *c*) as a biological wiring agent have at best approached 32% retained RC quantum efficiency. However, bottlenecks in cyt *c*-mediated electron transfer have not yet been fully elucidated. In this work, protein film voltammetry in conjunction with photoelectrochemistry is used to show that cyt *c* acts as an electron-funneling antennae that shuttle electrons from a functionalized rough silver electrode to surface-immobilized RCs. The arrangement of the two proteins on the electrode surface is characterized, revealing that RCs attached directly to the electrode via hydrophobic interactions and that a film of six cyt *c* per RC electrostatically bound to the electrode. We show that the additional electrical connectivity within a film of cyt *c* improves the high turnover demands of surface-bound RCs. This results in larger photocurrent onset potentials, positively shifted half-wave reduction potentials, and higher photocurrent densities reaching 100 $\mu\text{A cm}^{-2}$. These findings are fundamental for the optimization of bioelectronics that utilize the ubiquitous cyt *c* redox proteins as biological wires to exploit electrode-bound enzymes.

KEYWORDS: biosolar cells, biophotovoltaics, biophotoelectrochemistry, reaction center, cytochrome *c*



INTRODUCTION

Photosynthetic reaction centers (RCs) drive a photochemical charge separation that forms the energetic basis of most life on our planet. They do so with a near-unity quantum yield, transforming almost every absorbed photon into a displaced high-energy electron that drives biochemical processes within the organism. In the bacterial species *Rhodospirillum rubrum* (*Rb.*) *sphaeroides*, the key photovoltaic machinery is located within a 6 nm diameter transmembrane protein that is essentially a tractable nanoscale solar battery that can be removed from the bacterial cell and interfaced with man-made electrode materials. This has been achieved using a variety of strategies on metal electrodes,^{1–10} resulting in composite biohybrid photoelectrodes that support current densities of up to $\sim 400 \mu\text{A cm}^{-2}$. These half-cells form the platform for biophotovoltaics, which seek to exploit photosynthetic pigment proteins to develop alternative cheap and sustainable materials for solar energy conversion.^{11,12} In-depth summaries of progress in this field of RC-based biophotocathodes, including parallel work using photosystem I (PSI) and photosystem II (PSII) RCs, have been published in recent years.^{13–18}

A key aspect in the construction of biophotocathodes is the interface between the photovoltaic protein and the adjacent working electrode. Cytochrome *c* (cyt *c*) has been utilized as an electron-transfer (ET) element between electrodes and surface-bound enzymes, such as cyt *c* peroxidase,^{19,20} bacterial RCs,^{1,2,4,7} PSI,^{21,22} and PSII RCs,²³ supporting turnover rates approaching 71 s^{-1} and peak photocurrents of up to $416 \mu\text{A cm}^{-2}$.^{1,2,1,22,24–26,21,22,24–26} In comparison, net photocurrents of $322 \mu\text{A cm}^{-2}$ have been obtained for PSI connected to planar glassy carbon electrodes with engineered redox hydrogel films, but at much larger RC turnover rates of up to 335 s^{-1} that surpass those measured in vivo.¹⁶ This suggests that there is an untapped capacity for photocurrent output from biophotocathodes utilizing cyt *c* to aid ET to RCs.

The benefits of horse heart cyt *c*-mediated ET to bacterial RCs have been characterized on functionalized gold electrodes, resulting in photocurrent densities of a few $\mu\text{A cm}^{-2}$ and RC turnovers on the order of tens per second.^{1,4} PSI RCs have also

Received: April 13, 2017

Accepted: June 21, 2017

Published: June 21, 2017

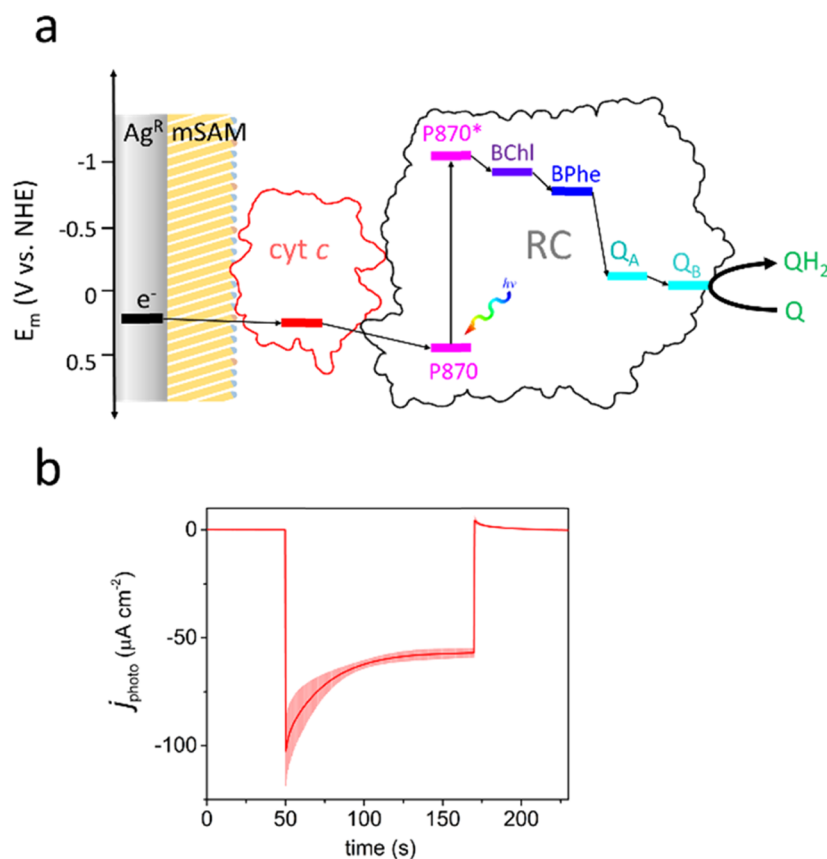


Figure 1. Biophotocathode schematic. (a) Proposed ET mechanism in the Ag^R|mSAM|cyt c|RC working electrode. (b) Photocurrent density response upon illumination beginning at 50 s and ending at 170 s at -50 mV vs Ag/AgCl.

been interfaced with working electrodes using cyt *c*, either to form multilayer systems that produce photocurrent densities on the order of a few $\mu\text{A cm}^{-2}$ on flat substrates, or up to $150 \mu\text{A cm}^{-2}$ on mesoporous substrates.^{21,22} These reports suggested that slow heterogeneous ET from the electrode to the cyt *c* limits RC turnover and thus photocurrents. Furthermore, both works suggest that the natural binding affinity between cyt *c* and the RC donor side allows cyt *c* to effectively act as a docking site for the oriented attachment of the RC onto immobilized molecules of cyt *c*.^{1,21}

Cytochromes are a class of heme-based proteins, some of which perform ET functions in both respiratory and photosynthetic electron transport chains.²⁷ Class I cytochromes of type *c* (cyt *c*) are defined by a covalently bound porphyrin, which is partially exposed to the solution through a crevice, and have an amino acid sequence that is heavily preserved such that the structure, electrochemical formal potential and binding properties are strongly conserved.^{27,28} This allows the substitution of cyt *c* between species as divergent as photosynthetic bacteria and mammals with negligible effects on enzyme turnover capacity.^{21,27,29} In purple photosynthetic bacteria, this protein (termed cyt *c*₂) is typically located in the periplasmic space or loosely attached to the periplasmic side of the membrane^{28,30} and shuttles electrons from the ubiquinol-cyt *c* oxidoreductase (cyt *bc*₁ complex) to the RC.³¹ There, it reduces the photo-oxidized primary electron donor bacteriochlorophyll pair (P⁺) produced by photochemical charge separation within the RC. This charge separation also produces a reduced, mobile ubiquinone species at the so-called Q_B site, which may be substituted by a water-soluble ubiquinone

analogue to optimize photocurrents in an RC-based photocathode.³²

Cyt *c* has long been at the heart of bio-electrochemistry, beginning with studies of mediated ET using soluble mediators such as 4,4 bipyridyl to direct ET on functionalized electrodes.^{33–37} The introduction of self-assembled monolayers (SAMs) on bare metal electrodes has enabled diffusionless voltammetry for more accurate and physiologically relevant characterization of cyt *c* ET phenomena by promoting strong binding of the electroactive cytochrome.^{38,39} The use of mixed SAMs (mSAMs) with various alkyl chain lengths and terminal functional groups has further increased the possibility of fine tuning the relevant parameters such as the magnitude of the electric field at the SAM–cyt *c* interface and the degree of protonation of the SAM, which has a strong impact on the ET properties of the bound protein.⁴⁰ This control may be advantageous in building bioelectrodes for designing faster ET or in improving protein binding.

In previous work, we have employed bare metal electrodes to bind both cyt *c* and RCs in a manner that results in significant photocurrents on the order of hundreds of $\mu\text{A cm}^{-2}$.^{2,22} However, cytochromes are known to bind to bare metals in a manner that hampers ET, not only limiting subsequent ET to the RC, but also making it difficult to electrochemically characterize the surface-adsorbed proteins and optimize ET bottlenecks. In the present work, we resolve these issues by functionalizing the bare metal surface using a mSAM that promotes effective SAM–cyt *c* binding, resulting in distinct faradaic currents (Figure S1), fast ET at the SAM–cyt *c* interface, as well as moderate RC loading.²⁴ This facilitated

protein film voltammetry (PFV) of the electroactive cyt *c*, which yielded key parameters such as the reversibility and rate of ET as well as the quantity of electroactive cytochrome. In conjunction with the recently coined technique “protein film photoelectrochemistry”,⁴¹ this has allowed us to simultaneously characterize the nature of cyt *c*-mediated ET and activity of the light-dependent enzyme. This is important for the design and full exploitation of a high-turnover enzyme/electrode system that uses cyt *c* as a biological wire. We find that optimal photocurrents of $\sim 100 \mu\text{A cm}^{-2}$ were obtained in low ionic strength buffers and high cyt *c* loading, resulting in a higher RC turnover. Furthermore, we deduced that cyt *c* mobility plays a crucial role in mediating ET between cyt *c* and the RC.

RESULTS

Construction of a Ag^RImSAM|Cyt c|RC Biophotocathode. An electrochemically roughened silver electrode (Ag^R) was chemically modified with a mSAM consisting of 11-mercaptoundecanol (MU) and 11-mercaptoundecanoic acid (MUA) in a ratio of 3:1 (see **Materials and Methods**). Purified *Rba. sphaeroides* RCs were subsequently drop-cast on the electrode, followed by cyt *c* to provide an electrical contact between the Ag^R and the RC primary electron donor bacteriochlorophylls P870 (Figure 1a). This coated electrode (termed Ag^RImSAM|cyt c|RC) was thoroughly rinsed in buffer solution to remove loosely bound complexes and placed in a three-electrode photoelectrochemical cell with 1.5 mM ubiquinone (UQ₀) as an electron acceptor.²² Upon photoexcitation with a 46 mW cm⁻² 870 nm LED, charge separation in the RC resulted in photo-oxidation of the primary electron donor (P⁺), which was reduced by transfer of an electron from a bound cyt *c*.³² Reduction of cyt *c* by the electrode resulted in a peak cathodic photocurrent of $\sim 100 \mu\text{A cm}^{-2}$ (Figure 1b), which translates to an apparent rate of RC turnover of $19 \pm 5 \text{ e}^- \text{ s}^{-1}$ (Table 1) or one electron every 53 ms.

Table 1. Performance of Ag^RImSAM|Cyt c|RC Electrodes

j_{photo}	$103 \pm 24 \mu\text{A cm}^{-2}$
Γ_{RC}	$53 \pm 12 \text{ pmol cm}^{-2}$
$\Gamma_{\text{cyt } c}$	$298 \pm 11 \text{ pmol cm}^{-2}$
$k_{\text{app,RC}}$	$19 \pm 5 \text{ e}^- \text{ s}^{-1} \text{ RC}^{-1}$
EQE_{app}	$0.31 \pm 0.1\%$
$\text{IQE}_{\text{app}}^a$	$13 \pm 2\%$

^aAssumes a contribution from reflection but not scattering.

Characterization of Cyt *c*-Electrode Binding. To characterize its binding affinity and loading, cyt *c* was titrated onto electrodes, and cyclic voltammograms (CVs) were recorded in a cyt *c*-free working buffer. A typical dataset is shown in Figure 2a. The electroactive surface-bound cyt *c* loading ($\Gamma_{\text{cyt } c}$) was measured from the area under the baseline-subtracted CV using eq 1³⁵

$$\left[\Gamma_{\text{cyt } c} = \frac{\text{area under CV peak}}{nFA\nu} \right] \quad (1)$$

where F is the Faraday constant (96485 C mol^{-1}), ν is the scan rate in V s^{-1} , A is the electrode area in cm^2 , and $n = 1$.

As shown in Figure 2b, the value of $\Gamma_{\text{cyt } c}$ increased with the concentration of drop-casted cyt *c* until saturation at $30 \mu\text{M}$ cyt *c*, at which point $\Gamma_{\text{cyt } c}$ reached a maximum of approximately 300 pmol cm^{-2} (Figure 2b). When RCs were preloaded on the

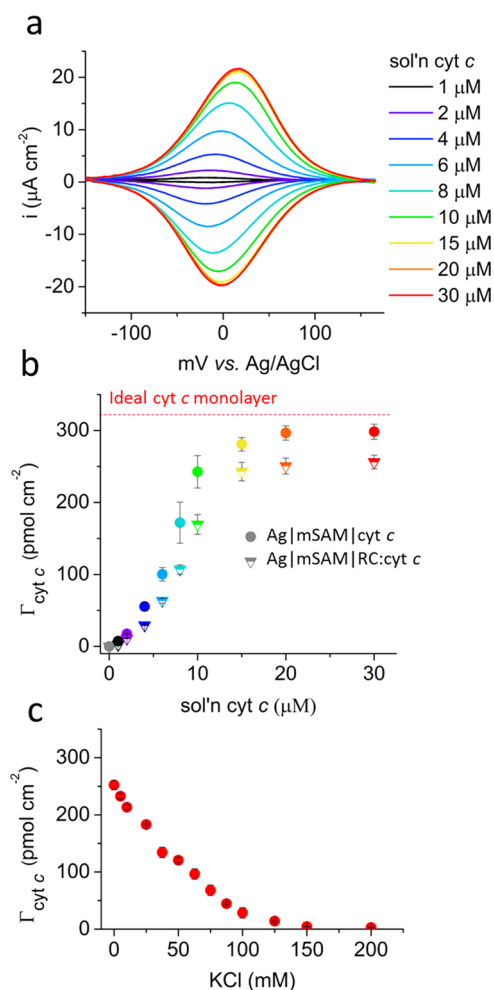


Figure 2. Cyt *c*-electrode-binding affinity. (a) Baseline-subtracted CVs of a Ag^RImSAM electrode as a function of solution cyt *c* concentration. (b) $\Gamma_{\text{cyt } c}$ derived from baseline-subtracted peak integration of plot (a) on electrodes prefunctionalized with RCs (Ag^RImSAM|cyt c|RC) and without RCs (Ag^RImSAM|cyt *c*). The preloaded electrode had a Γ_{RC} of 53 pmol cm^{-2} . (c) $\Gamma_{\text{cyt } c}$ as a function of ionic strength. The loading measurements were taken after a 2 min incubation in the presence of KCl at the concentrations indicated. KCl was not present in the cell during CV measurements. Error bars represent 1 standard deviation, with $n = 4$.

electrode, a maximum cyt *c* loading of 280 pmol cm^{-2} was observed (Figure 2b). To characterize the nature of the cyt *c* adsorption, the ionic strength of the working buffer was increased. It was found that cyt *c* was completely desorbed above 150 mM KCl (Figure 2c), indicating that the cyt *c*-mSAM interaction is electrostatic in nature. This was in agreement with previous results on a pure and mixed MUA SAM.⁴²

The experimentally determined $\Gamma_{\text{cyt } c}$ maximum (300 pmol cm^{-2}) compared well with the theoretical maximum of 320 pmol cm^{-2} . The theoretical $\Gamma_{\text{cyt } c}$ maximum was estimated using the reported loading of 15 pmol cm^2 for an ideally packed cyt *c* monolayer,³⁵ which is in close agreement with the experimentally determined $\Gamma_{\text{cyt } c}$ on flat Au-MUA.⁴² This is also similar to the reported $\Gamma_{\text{cyt } c}$ on a mSAM of the same composition used in this work.²¹ This ideal loading was multiplied by a reported 21-fold surface area increase for a rough silver electrode versus a flat silver electrode to obtain 320 pmol cm^{-2} .^{36,36}

The two $\Gamma_{\text{cyt } c}$ curves in Figure 2b have a similar shape and cyt *c* concentration at which $\Gamma_{\text{cyt } c}$ was half-maximal (Figure 2b), suggesting that the binding affinity of the electrode for cyt *c* was not affected by the presence of RCs. However, the maximum value of $\Gamma_{\text{cyt } c}$ was decreased by approximately 6.7% in the presence of RCs (Figure 2b), indicating some competition with RCs displacing the available surface binding sites for cyt *c*.

Closer examination of the CV traces in Figure 2a revealed a positive shift in the formal potential ($E^{\circ'}_{\text{cyt } c}$) and increase in the peak width half-maximum (PWHM) as $\Gamma_{\text{cyt } c}$ increases (plotted in Figure S2). Clark et al. have suggested that a broader PWHM stems from a more heterogeneous population of electroactive cyt *c* forms with variation in formal potentials. This heterogeneity could arise from favorable stabilization of the oxidized form of cyt *c* on the intrinsically heterogeneous surface and/or adsorption-induced heterogeneity arising from steric exclusion.⁴²

Characterization of RC-Electrode Binding. To determine the nature of RC adsorption on the electrode surface, Ag^RImSAM|cyt *c*|RC electrodes were exposed to high ionic strength buffer (1 M KCl) or detergent-containing buffer (1% β -dodecyl maltoside (DDM)) and photocurrent densities compared (j_{photo}) (Figure 3). Upon treatment with 1 M KCl

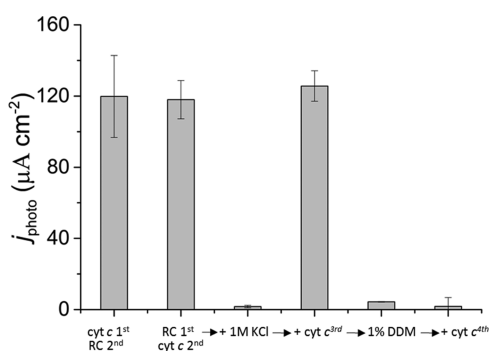


Figure 3. Binding of RCs to the electrode. Peak photocurrents from Ag^RImSAM|cyt *c*|RC electrodes, whereby the cyt *c* was drop-casted first, followed by the RC, and vice versa. The latter electrode was then sequentially treated with 1 M KCl, drop-casted with cyt *c* (50 μM for 5 min), treated with 1% DDM and again drop-cast with cyt *c*. This last incubation (cyt *c* fourth) step ensured the cyt *c* monolayer was re-established, and that any photocurrent decrease attributed to RC desorption. Each step was interceded with rinsing in milli-Q for 15 min. Error bars represent standard deviation, $n = 4$.

followed by drop-casting with cyt *c*, no significant loss of photocurrent was observed, indicating that the RC was not adsorbed to the electrode through electrostatic interactions. However, upon treatment with 1% DDM, the photocurrent disappeared indicating that hydrophobic interactions between RC and electrode are dominant for binding. An absorption spectrum of the desorbed RC (see Materials and Methods) revealed a Γ_{RC} of $53 \pm 12 \text{ pmol cm}^{-2}$. Drop-casting cyt *c* on the electrode first and RC second resulted in a similar j_{photo} , suggesting that preloaded cyt *c* does not play a docking role in binding additional RCs to the electrode, in contrast to other reports¹. Furthermore, incubation of cyt *c* first and RCs second electrodes in 1 M KCl, which disrupts both solution RC–cyt *c*²⁹ and cyt *c*–electrode binding (see above), resulted in negligible desorption of RCs, further confirming that the RC was docked directly to the electrode and not via cyt *c*.

An estimated Γ_{RC} of 53 pmol cm^{-2} corresponds to approximately 45% surface coverage, assuming a spherical RC with a diameter of 6 nm. Assuming that the other 55% is covered by cyt *c*, one would expect a $\Gamma_{\text{cyt } c}$ of $\sim 175 \text{ pmol cm}^{-2}$ based on the dimensions of a molecule of cyt *c*. However, a maximum $\Gamma_{\text{cyt } c}$ of 280 pmol cm^{-2} was measured on the Ag^RImSAM|cyt *c*|RC electrode. This discrepancy suggests that the RC and cyt *c* may coadsorb. Such an effect was not apparent in the binding affinity of cyt *c* as determined by titration (Figure 2b), which showed no significant difference in cyt *c* binding affinity to RC-adsorbed or RC-free electrodes; however, we cannot exclude the fact that the electrode–cyt *c* and RC–cyt *c* binding affinities are very similar and not distinguishable by this method. It has been shown that the isolated RC can bind (up to) 24 molecules of cyt *c*,⁴³ and the PSI RC has been shown to promote the coadsorption of electroactive cyt *c* to form multilayers on electrode surfaces.²¹ It is likely that we have a similar semi-multilayer architecture on our electrodes.

Effect of cyt *c* Loading on Photocurrent and Onset Potential. To characterize the effect of a shifted cyt *c* formal potential on RC turnover, as measured by photocurrent, photocatalytic voltammograms (pCV) were recorded at low, medium, and high $\Gamma_{\text{cyt } c}$ (Figure 4c). The pCV can be described as a Nernstian catalytic wave, whose half-wave potential (E_{hw}) allows identification of the midpoint potential of the redox center that mediates ET between the electrode and the RC.⁴⁴ E_{hw} was determined by taking the first derivative of the pCV, as described in Figure S3. From this analysis, it was clear that E_{hw} (Figure 4c) was close to the $E^{\circ'}_{\text{cyt } c}$ (Figure 4a), thus identifying cyt *c* as the redox center mediating the ET between the SAM and the RC.⁴⁴ However, the total magnitude of the E_{hw} shift was $43.5 \pm 5 \text{ mV}$, 20 mV more than the corresponding shift in $E^{\circ'}_{\text{cyt } c}$. This nonproportional shift became more pronounced at lower light intensities (see Figure S4).

To determine whether the faster heterogeneous electrode to cyt *c* ET played a role in this nonproportional E_{hw} shift, the cyt *c*–Ag^RImSAM quasi-reversible ET rate constant (k_{ET}) was determined via the Laviron method.⁴⁵ k_{ET} was found to be 41.8 ± 1.9 , 42.7 ± 1.9 , and $44.2 \pm 2.5 \text{ s}^{-1}$ for high, medium, and low $\Gamma_{\text{cyt } c}$, respectively (Figure S5). The lack of a significant difference in k_{ET} between cytochrome loadings indicates that a larger k_{ET} between the various subpopulations of electroactive cyt *c* does not play a role in the shift of E_{hw} or the higher photocurrent at high cyt *c* loading. To determine whether the measured electroactive cyt *c* consisted of multilayers, we ensured the peak faradaic current ($i_{\text{p-}}$) remained linear with respect to scan rates up to 15 V s^{-1} (Figure S8). This suggests that cyt *c* is in close ET contact with the working electrode, or that the scanning speed had not exceeded the rate of cyt *c* self-exchange (k_{ex}) between potential cyt *c*-multilayers, as the $i_{\text{p-}}$ would otherwise drop off at higher scan rates, as shown previously.⁴⁶

The nonproportional shift in E_{hw} relative to the shift in $E^{\circ'}_{\text{cyt } c}$ suggests that ET to the RC is more effective at high cyt *c* loading, requiring a lower electrode overpotential (the driving force to sustain the photocatalytic activity of the RC) that is not solely due to the positive shift in the formal potential of weakly bound molecules of cyt *c*. We hypothesize that this arises from the transition of a sub-monolayer of relatively isolated cyt *c* molecules to an electrically interconnected cyt *c* layer as $\Gamma_{\text{cyt } c}$ increases (see Figure S6). This would effectively enable the cyt *c* layer to act as an electrical capacitor, harvesting electrons from the electrode, storing them, and shuttling them to the RC upon

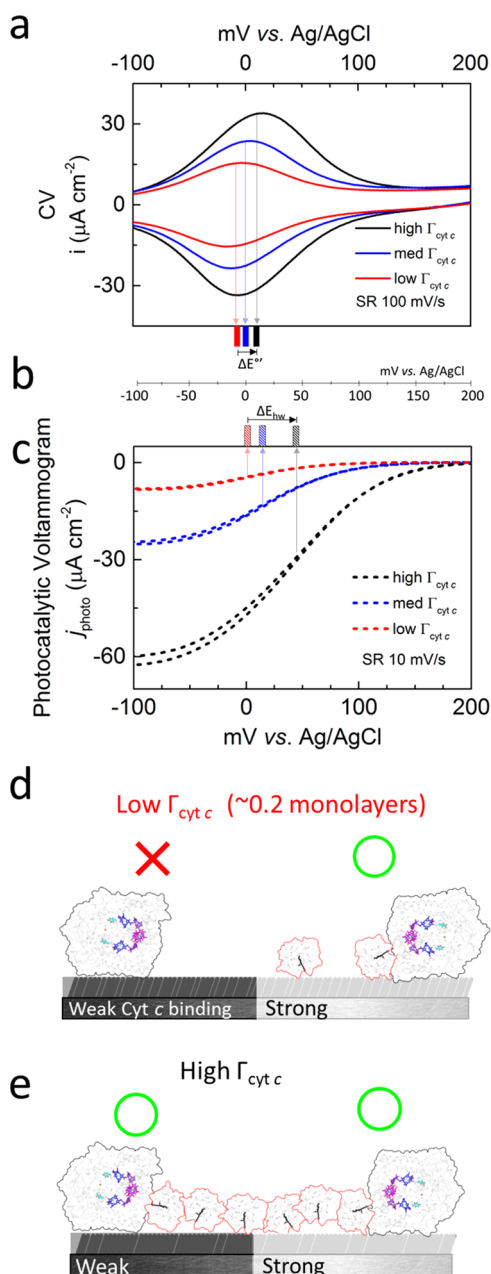


Figure 4. Effects of cyt *c* loading on electrode performance. (a) Cyclic voltammograms at low (292 pmol cm⁻²), medium (155 pmol cm⁻²), and high (55 pmol cm⁻²) $\Gamma_{\text{cyt}c}$. (b) CV $E'_{\text{cyt}c}$ vs E_{hw} from the pCV in full vs striped bars. (c) pCVs recorded under forced convection at a sweep rate of 10 mV s⁻¹. (d) Schematic depicting the electrode surface at low $\Gamma_{\text{cyt}c}$. (e) Schematic depicting the electrode surface at high $\Gamma_{\text{cyt}c}$.

demand. A high $\Gamma_{\text{cyt}c}$ would likely (i) facilitate lateral cyt *c*–cyt *c* exchange, thanks to smaller cyt *c*–cyt *c* distances, (ii) increase cyt *c*–electrode contact points per RC, and (iii) increase the probability of cyt *c*–RC contacts (Figure 1a, yellow, green, and blue arrows respectively).

The larger photocurrents may also be aided by the additional mobility of weakly bound cyt *c* molecules that exist under high $\Gamma_{\text{cyt}c}$. Based on the model depicted in Figure 1, the electrical communication between the RC and the electrode can be assisted by a massive and unprecedentedly reported reorientation of cyt *c* involving the repositioning of the heme crevice from the mSAM to the electron entry site of the RC. Regardless

of the precise mechanism, it is clear that a high $\Gamma_{\text{cyt}c}$ results in a larger photocurrent and a more positive onset potential, amenable to the optimization of the open-circuit voltage and current in a biophotovoltaic device.

The observed shift in E_{hw} with $\Gamma_{\text{cyt}c}$ provides evidence against a previously suggested RC–cyt *c* interaction for wiring of the RC to the electrode surface,¹ as this would predict no significant variation in E_{hw} at low, medium, or high cyt *c* loading. This further implies that the probability of RC wiring is driven by the local electrode environment in which it is bound, be it through strongly or weakly binding the cyt *c* species (Figure 4d). We speculate that under high ionic strength (low $\Gamma_{\text{cyt}c}$), cyt *c* attaches to regions that strongly bind cyt *c* and wires any surrounding RCs to the electrode, resulting in a photocurrent (Figure 4, green circles), but RCs bound to regions that weakly bind cyt *c* do not contribute to the current (Figure 4d).

Higher $\Gamma_{\text{cyt}c}$ Boosts RC Turnover. To further investigate the effect of $\Gamma_{\text{cyt}c}$ on RC turnover, photocurrents were measured as a function of irradiance for electrodes with low, medium, and high cyt *c* loadings. Under increasing irradiance, the photocurrent approached a plateau, indicating a rate limitation in the ET cascade (Figure 5). The peak photocurrent

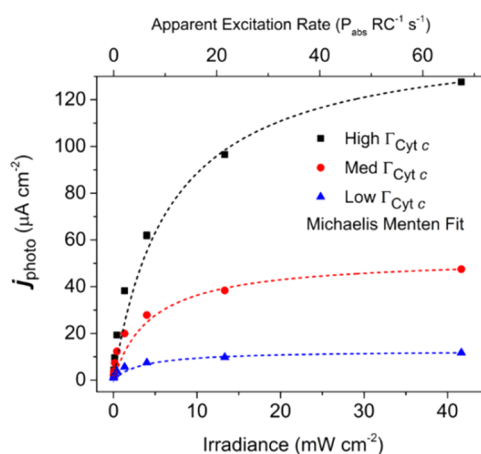


Figure 5. Improvement of RC turnover at high $\Gamma_{\text{cyt}c}$. Photocurrents measured as a function of irradiance at high, medium, and low $\Gamma_{\text{cyt}c}$ are plotted in black, red, and blue, respectively. Michaelis–Menten fits are shown as dashed lines, with $R^2 > 0.999$. Error bars represent standard deviation with $n = 4$. The photon absorption rate of the RC as a function of irradiance is shown on the top axis.

decreased with decreasing $\Gamma_{\text{cyt}c}$ but the steepness of the initial slope was larger in relative terms, indicating that the photocurrent also plateaued more quickly with decreasing $\Gamma_{\text{cyt}c}$.

The data were fitted with a Michaelis–Menten enzyme–single substrate model, where it was assumed that the measured photocurrent is directly proportional to RC turnover, and the substrate term was the light, or more specifically, the rate of photons absorbed.²² In this model, it was assumed that the only rate limitation was the cyt *c*–mediated ET on the donor side of the RC. This was valid because ET was optimized on the RC acceptor side by using a sufficiently high concentration of UQ₀ (1.5 mM) in the buffer solution⁴⁷ and a rotating disc electrode to mitigate limitations imposed by quinone diffusion, as reported in previous work. In this model, the apparent V_{max} (maximum photocurrent) was a function of both the number of wired RCs and the RC turnover rate. From V_{max} alone, it was

not possible to discern whether the individual RCs that are wired by cyt *c* are rate limited by cyt *c* ET. However, the initial steepness of the curve at low irradiance levels in the experimental data (Figure 5) is an intrinsic parameter of the population of RCs that are wired. Thus, the apparent RC photon absorption rate at which the photocurrent is half-saturated ($RC_{abs\ 1/2}$) was used to compare the RC turnover capacity at different values of $\Gamma_{cyt\ c}$ (see Materials and Methods for calculation of this parameter). The value of $RC_{abs\ 1/2}$ doubled from a low to a high cyt *c* loading, suggesting that the RC turnover was indeed less encumbered at a higher $\Gamma_{cyt\ c}$ (Table 2). However, the photocurrents plateaued at a photon

Table 2. Parameters from Michaelis–Menten Fits of Photocurrent Density as a Function of Irradiance^a

	V_{max} (i_{peak})	k_m ($V_{max}/2$)	$RC_{abs\ 1/2}$ ($n_{abs}\ s^{-1}\ RC^{-1}$)
low $\Gamma_{cyt\ c}$	12 ± 0.2	3.5 ± 0.5	5.6 ± 0.8
med $\Gamma_{cyt\ c}$	52 ± 0.7	4.5 ± 0.5	7.2 ± 0.8
high $\Gamma_{cyt\ c}$	150 ± 2	6.7 ± 0.5	10.7 ± 0.8

^aAdjusted R^2 for all fits is >0.99.

absorption rate of only $150\ s^{-1}\ RC^{-1}$, which falls far below the maximum turnover rate of $2300\ s^{-1}$ that RCs have been shown to exhibit in solution, using the same redox mediators, UQ₀, and equine cyt *c*.²⁹

Cyt *c* Mobility Is Essential for ET to the RC. Ions are proposed to play an important role in screening charges to facilitate cyt *c*–RC unbinding, reaching an optimal value of 40 mM NaCl.²⁹ To investigate the role of ionic strength in our electrode-immobilized system, photocurrents were recorded as a function of KCl concentration in the buffer solution (Figure 6a, black). The photocurrent was found to peak at 10 mM KCl, which is somewhat lower than the value of 40 mM reported in solution studies. However, concomitant desorption of cyt *c* from the electrode surface (Figure 6a, red) skews the real optimal ionic strength of cyt *c*-mediated ET to the RC on the electrode surface. Regardless, RC–cyt *c* behavior on the electrode was similar to that in solution, suggesting that electrostatic screening by ions plays a role in facilitating binding and unbinding of the RC–cyt *c* complex at the electrode surface. It is also likely that electrostatic screening conferred by the higher ionic strength plays a role in facilitating cyt *c* mobility, as this has already been shown to lead to cyt *c* desorption from the electrode surface. The mobility may assist in the cyt *c* reorientation needed to position the heme crevice from the mSAM–solution interface to face and transfer an electron to the RC.

To further investigate whether cyt *c* translation or rotational mobility played a role in ET, the cross linkers 1-ethyl-3-(3-dimethylaminopropyl) carbodiimide (EDC) or glutaraldehyde (GLUT) were applied to Ag¹⁰ImSAM/cyt *c*/RC electrodes, as described previously.^{48,49} EDC is a zero-length cross-linker that links amines, which are abundant on the RC and cyt *c*, and carboxylic acids, which are abundant on the SAM and the RC. It would therefore be expected to cross-link the cyt *c* to the RC and irreversibly bind the complex to the electrode surface. Glutaraldehyde is a four-carbon bifunctional cross-linker that targets amines and is expected to lock the cyt *c* layer and interacting cyt *c*-RCs in place, but not cross-link these to the electrode. With both cross linkers, a sub-monolayer of cyt *c* remained on the electrode after rinsing in 1 M KCl, indicating successful preservation of covalently bound electroactive cyt *c*

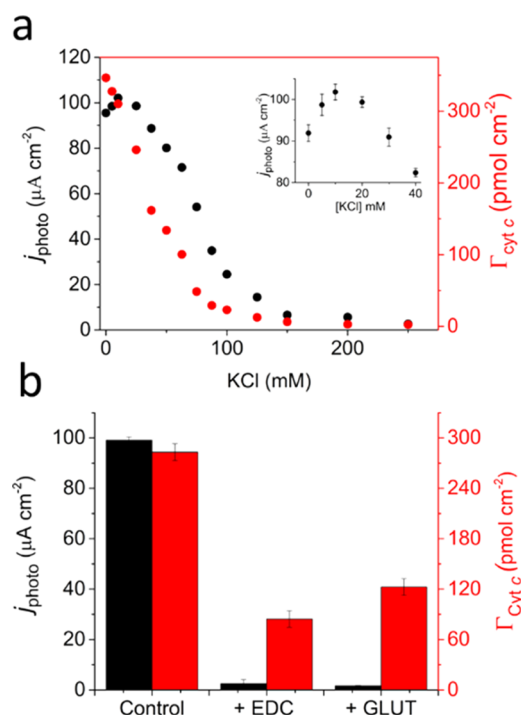


Figure 6. Effect of cyt *c* binding and mobility on photocurrent. (a) Photocurrent density as a function of ionic strength (left axis, black) and $\Gamma_{cyt\ c}$ (right axis, red). (b) Effect of cross-linking Ag¹⁰ImSAM/cyt *c*/RC electrodes with carbodiimide (EDC) and glutaraldehyde (GLUT) on photocurrent (black) and $\Gamma_{cyt\ c}$ (red).

on the electrode surface (Figure 6b). However, both cross-linking treatments resulted in an almost complete loss of photocurrent. This profound inhibition of photocurrent, despite ET from electrode to surface-bound cyt *c*'s, was clear indication that mobility of the protein plays a role in mediating ET from the cyt *c* to the RC. This is in good agreement with previous conclusions that the rate of many protein–protein ETs is limited, or gated, by conformational reorientation.⁵⁰ To ensure that cross-linking did not deactivate the RC itself, fresh RCs were adsorbed to the cross-linked RC–cyt *c* electrodes. We speculated that if the cross-linking and denaturation of the RC protein was the cause for photocurrent decrease, addition of uncross-linked RCs onto the electrode would restore photocurrents; however, this was not the case (data not shown). Conversely, addition of cyt *c* after cross-linking did restore some of the photocurrent in the EDC cross-linked electrode, and the RC functionality was probed using the wavelength-dependent action spectrum. The photocurrent response mirrored that of the native RC solution spectra, indicating a native RC conformation after cross-linking in EDC (see Figure S8). However, no photocurrent response was shown for the GLUT cross-linked electrode both before and after additional cyt *c* incubation, perhaps due to both RC denaturation and restriction of cyt *c* mobility.

DISCUSSION

Physiological Relevance. The mechanism of cytochrome ET between transmembrane proteins in biological ET chains has been proposed to involve one or a combination of three possible processes: (1) complete three-dimensional diffusion whereby the cytochrome detaches from the membrane/protein surface into bulk solution to diffuse to the next membrane-

embedded redox partner, (2) two-dimensional diffusion on the membrane surface via rotational mobility and/or lateral diffusion, and (3) an immobilized film configuration in which the cytochromes act as a network of relay centers between transmembrane redox proteins.⁵¹ Self-exchange rates (k_{ex}) for horse heart cyt *c* of 10^3 s^{-1} at a low ionic strength (0.1 M NaCl) and 10^4 s^{-1} at a high ionic strength (1 M NaCl) have been determined.⁵² However, whether lateral ET occurs in a monolayer of cyt *c* on a membrane surface is not known, but has been shown for three-dimensional multilayers.⁴⁶

When adsorbed to a negatively charged SAM in man-made systems, cyt *c* undergoes a redox shift of -45 mV relative to the solution value, which is comparable to that reported for cyt *c* bound to biological membranes due to stabilization of the cyt c^{3+} form.³⁵ Bowden et al. have suggested that surfaces with a higher defect density, resulting in irregularities in the chemical and topographical texture of the mSAM on flat gold, more closely resemble the natural membrane-protein environment and binds ET proteins with optimal electronic coupling.⁴⁰ If we also consider that the rough silver topography promotes better protein adsorption versus a smooth topology,³³ it may reveal why the $\text{Ag}^{\text{R}}\text{ImSAM}$ is such a good candidate for binding cyt *c* and transmembrane proteins with fast ET, despite the added tunneling barrier inferred by the 11-carbon alkyl chain.

In the absence of precise information on the structure of the RC–cyt *c* complex on the electrode surface, it is not possible to decisively discriminate between the different models for ET on our electrodes. However, our data support the model of a cyt *c* film on the membrane surface, with rotational and perhaps lateral mobility playing a role in ET, as illustrated in the TOC.

CONCLUSIONS

This work shows that cyt *c* electrostatically binds and saturates a $\text{Ag}^{\text{R}}\text{ImSAM}$ surface, forming a full electroactive monolayer. In contrast, the RC adsorbs on the electrode via hydrophobic regions that are normally embedded in the membrane interior. The finding that high cyt *c* loading yields larger photocurrents and more positive onset potentials is important for improving the short-circuit currents and open-circuit voltages of cyt *c*-based biophotovoltaic systems. We suggest this is due to an interconnected cyt *c* layer, which acts as an electron-funneling antenna and electron-storing capacitor for delivery of electrons to the RC. Our data show that cyt *c* mobility is crucial for ET from the cyt *c* to the surface-bound RCs, likely due to reorientation of the heme group from the electrode surface for lateral cyt *c*–cyt *c* exchange, or toward the photo-oxidized RC primary electron donor cofactors. Finally, we have obtained definitive evidence on the central role of cyt *c*-mediated ET to RCs immobilized on electrodes. We show the cyt *c* indeed gates ET to the RC, via the shift in the half-wave potential that is consistent with the positive shift in cyt *c* formal potential.

Collectively, these findings suggest that further improving both the coverage and the mobility of surface-adsorbed cyt *c* will improve the electrical communication between the electrode and the RC, thus enhancing the photocurrent and onset potential. The maximum RC turnover rates achieved in the present study ($19 \text{ e}^- \text{ s}^{-1}$) are still orders of magnitude lower than those determined for solubilized RCs ($1000 \text{ e}^- \text{ s}^{-1}$), showing that cyt *c*-mediated ET, even when optimized to the extent described above, is still insufficient to meet the demands of RC turnover. Thus, it is necessary to further engineer the cyt *c* or substitute it with a more efficient ET mediator that is better suited to interface the RC to the electrode.

MATERIALS AND METHODS

Materials. Horse heart cyt *c*, 2,3-dimethoxy-5-methyl-*p*-benzoquinone (UQ_0), MUA, and MU were purchased from Sigma-Aldrich. Milli-Q water (Millipore, MA) was used in all preparations and procedures.

RC Isolation and Purification. A strain of *Rba. sphaeroides* lacking light harvesting complexes and expressing His-tagged wild-type RCs was constructed and purified by nickel affinity chromatography, as described previously.⁴⁷

Electrode Construction. Planar disc 3 mm Ag working electrodes (Metrohm Autolab BV, Utrecht, Netherlands) were mechanically polished with Al_2O_3 lapping films of successively finer grain sizes of 5, 3, and 1 μm (Thor Labs), followed by rinsing of the electrode with Milli-Q water after each polishing step. An electrochemical roughening procedure was then applied, as described previously.⁵³ Roughened silver electrodes (Ag^{R}) were then incubated for at least 48 h in a solution of 1.25 mM MUA and 3.75 mM MU in 100% ethanol at room temperature in the dark. The resulting $\text{Ag}^{\text{R}}\text{ImSAM}$ working electrodes were tested for quality by running CVs in 5 mM potassium phosphate (pH 5.0) in the presence of oxygen from -300 to $+300 \text{ mV}$ versus Ag/AgCl to check the SAM quality/full formation. A good SAM did not show any oxygen reduction signal or Ag oxidation at potentials up to -350 mV versus Ag/AgCl.

After thorough rinsing in ethanol and Milli-Q, $\text{Ag}^{\text{R}}\text{ImSAM}$ electrodes were drop-cast with a solution of 288 μM RC in 20 mM Tris (pH 8.0)/0.04% DDM for 15 min, rinsed, then drop-cast with a solution of 30 μM cyt *c* in 5 mM phosphate (pH 7.0) for 5 min, unless otherwise specified. The resulting $\text{Ag}^{\text{R}}\text{ImSAM|cyt } c\text{RC}$ electrodes were then inserted into a photoelectrochemical cell fitted with a Ag/AgCl/3 M KCl reference electrode and a platinum counter electrode (both from Metrohm Autolab) in a working solution of 1.5 mM UQ_0 in 5 mM phosphate (pH 7.0). A PGSTAT128N potentiostat (Metrohm Autolab) was used to control the three-electrode cell, with a bias potential of -50 mV versus Ag/AgCl being applied, unless otherwise specified. The working electrode was illuminated with an 870 nm LED (LED 870-66-60, Roithner Lasertechnik) with an irradiance of 46 mW cm^{-2} at the electrode surface.

Cyt *c* Titrations. Cyt *c* was titrated onto the electrode by immersion in a room temperature solution containing a defined concentration of cyt *c* for 2 min, followed by two sets of rinsing in 5 mM phosphate (pH 7.0). Rinsed electrodes were then placed into the three-electrode cell.

Calculation of External and Internal Quantum Efficiency, and RC Photon Absorption rate. External quantum efficiency (EQE = charge carriers/incident photons) was calculated using the following equation

$$\text{EQE} = \frac{j_{\text{photo}}}{q\phi_{\text{inc}}} \quad (2)$$

where j_{photo} is the peak photocurrent density ($\text{C s}^{-1} \text{ cm}^{-2}$), q is the elementary charge of an electron ($1.602 \times 10^{-19} \text{ C}$), and ϕ_{inc} is the incident photon flux ($N_p \text{ cm}^{-2} \text{ s}^{-1}$) on the electrode surface (N_p is the number of photons). Φ_{inc} of the LED used, centered at 868 nm with a FWHM of 36.5 nm, was calculated to be $3.99 \times 10^{17} N_p \text{ cm}^{-2} \text{ s}^{-1}$ (see Figure S7 for the broadband $\phi_{\text{inc}} \text{ nm}^{-1}$). This assumed 100% reflection on the silver surface, but ignored any light absorption enhancement from scattering and other plasmonic effects.

Internal quantum efficiency (IQE = charge carriers/absorbed photons) was calculated using

$$\text{IQE}_{\text{app}} = \frac{j_{\text{photo}}}{q\phi_{\text{abs}}} \quad (3)$$

where the total number of absorbed photons (Φ_{abs}) corresponded to the following

$$\phi_{\text{abs}} = \sum_{\lambda=400 \text{ nm}}^{1000 \text{ nm}} (1 - T_{\lambda}) * \phi_{\text{inc } \lambda} \quad (4)$$

where $(1 - T_\lambda)$ corresponds to the percentage absorption of the RC layer at wavelength λ , taken from the RC loading determined as described below. All calculations were carried out in steps of 1 nm. Figure S6 shows full spectrum plots of the WE transmittance, LED-generated incident photon flux, total number of absorbed photons (Φ_{abs}), and photon absorption rate per RC.

Determination of RC Loading, Turnover, and Photon Absorption Rate. Upon completion of photocurrent measurements, each working electrode was inserted into a 500 μL microcentrifuge tube containing 250 μL of 1% β -DDM in 5 mM phosphate (pH 7.0), the tube was vortexed for 30 s in the dark, followed by mild sonication for 30 s. The electrode was removed, and the absorbance spectrum of the solution containing extracted RCs was recorded. The loading of RC complexes on the electrode (Γ_{RC} , mol cm^{-2}) was calculated using an extinction coefficient of 288 $\text{mM}^{-1} \text{cm}^{-1}$ at 803 nm.⁵⁴ The apparent RC turnover rate (k_{app}) was determined using

$$k_{\text{app}} = \frac{j_{\text{photo}}}{nF \Gamma_{\text{RC}}} \quad (5)$$

where j_{photo} is the photocurrent flux in A cm^{-2} , Γ_{RC} is the RC loading in mol cm^{-2} , F is the Faraday constant (96 485 C mol^{-1}), and n is the number of electrons per cyt c turnover (i.e., 1). The apparent RC turnover rates assume the quantity and functionality of wired RCs is 100%.

Determination of Cyt c Loading. Baseline CVs of $\text{Ag}^{\text{R}}\text{ImSAM}$ electrodes were run from -150 to $+175$ mV versus Ag/AgCl at a scan rate of 250 mV s^{-1} in 5 mM phosphate (pH 7.0) before incubation in cyt c . After incubation in buffer at a specified cyt c concentration (see above), CVs were recorded at 250 mV s^{-1} and the baseline subtracted. The total charge transferred during the cathodic or anodic sweep was used to calculate the Γ cyt c concentration using eq 1. The typical magnitudes of the cathodic and anodic peaks were nearly identical, indicating a reversible ET process, whereby the number of electrons going into the cyt c layer was similar to that of the ones going out.

Catalytic Wave. For catalytic wave experiments, $\text{Ag}^{\text{R}}\text{ImSAM}\text{IRC}$ electrodes were incubated in a solution containing 2, 8, or 30 μM cyt c for 2 min to achieve a low, medium, or high loading of cyt c , respectively. The catalytic wave was recorded using a 3 mm Autolab rotating disk electrode at a scan rate of 10 mV s^{-1} , under constant rotation (500 rpm) and in the presence of a high concentration of UQ0 (1 mM) to ensure the diffusion of the acceptor side mediator was not rate limiting for the photocurrent. E_{hw} was determined by identifying the inflection point, or peak of the derivative, of the pCV as described previously,²⁵ and as illustrated in Figure S3.

Cross Linking. EDC cross linking was achieved by a 30 min incubation of a $\text{Ag}^{\text{R}}\text{ImSAM}\text{cyt } c\text{IRC}$ electrode in 5 mM EDC/5 mM phosphate (pH 7.0)/30 μM cyt c , as described previously.⁴⁸ Glutaraldehyde cross linking was achieved by incubation of electrodes for 2 h in 0.1% (w/v) glutaraldehyde/5 mM phosphate (pH 7.5). In both procedures, incubation was followed by thorough rinsing of the electrode in 5 mM phosphate (pH 7.5) before measurement.

■ ASSOCIATED CONTENT

Supporting Information

The Supporting Information is available free of charge on the ACS Publications website at DOI: 10.1021/acsami.7b03278.

CVs, correlation of CV peak width half-maximum with loading, pCV midpoint potential determination, ET rate constant determination via Laviron method, IQE calculation, and wavelength-dependent EQE determination (PDF)

■ AUTHOR INFORMATION

Corresponding Author

*E-mail: r.n.frese@vu.nl

ORCID

Vincent M. Friebe: 0000-0002-4277-8473

David J. K. Swainsbury: 0000-0002-0754-0363

Raoul N. Frese: 0000-0001-8243-9954

Present Address

[§]Department of Molecular Biology and Biotechnology, University of Sheffield, Firth Court, Western Bank, Sheffield S10 2TN, U.K. (D.J.K.S.).

Author Contributions

D.J.K.S. and M.R.J. provided purified RC complexes. V.M.F. performed photochronoamperometry and PFV. V.M.F., D.M., and R.N.F. designed and supervised the experiments. V.M.F., M.R.J., and R.N.F. wrote the manuscript. All authors discussed the results and commented on the manuscript.

Funding

M.R.J. and D.J.K.S. acknowledge support from the Biotechnology and Biological Sciences Research Council of the U.K. (project BB/I022570/1). R.N.F. acknowledges support from the Dutch Science Foundation NWO for a vidi grant, and D.M. for a veni grant (no. 722.011.003). Molecular graphics were performed with the UCSF Chimera package. Chimera is developed by the Resource for Biocomputing, Visualization, and Informatics at the University of California, San Francisco (supported by NIGMS P41-GM103311).

Notes

The authors declare no competing financial interest.

■ ABBREVIATIONS

cyt c , cytochrome c ; RC, reaction center; bPV, biophotovoltaics; PSI, photosystem I; ET, electron transfer; mSAM, mixed self-assembled monolayer; Ag^{R} , electrochemically roughened silver working electrode; CV, cyclic voltammogram; pCV, photocatalytic voltammogram; $\Gamma_{\text{cyt } c}$, cyt c loading; Γ_{RC} , RC loading; MU, mercaptoundecanol; MUA, mercaptoundecanoic acid; UQ₀, ubiquinone-0; KCl, potassium chloride; DDM, β -dodecyl maltoside; k_{ex} , self-exchange rate; $\text{RC}_{\text{abs } 1/2}$, apparent RC photon absorption rate at which photocurrent is half-saturated

■ REFERENCES

- (1) Yaghoubi, H.; Li, Z.; Jun, D.; Lafalce, E.; Jiang, X.; Schlaf, R.; Beatty, J. T.; Takshi, A. Hybrid Wiring of the *Rhodospira rubra* Reaction Center for Applications in Bio-Photoelectrochemical Solar Cells. *J. Phys. Chem. C* **2014**, *118*, 23509–23518.
- (2) Den Hollander, M. J.; Magis, J. G.; Fuchsenger, P.; Aartsma, T. J.; Jones, M. R.; Frese, R. N. Enhanced Photocurrent Generation by Photosynthetic Bacterial Reaction Centers through Molecular Relays, Light-Harvesting Complexes, and Direct Protein-Gold Interactions. *Langmuir* **2011**, *27*, 10282–10294.
- (3) Magis, G. J.; den Hollander, M. J.; Onderwaater, W. G.; Olsen, J. D.; Hunter, C. N.; Aartsma, T. J.; Frese, R. N. Light Harvesting, Energy Transfer and Electron Cycling of a Native Photosynthetic Membrane Adsorbed onto a Gold Surface. *Biochim. Biophys. Acta, Biomembr.* **2010**, *1798*, 637–645.
- (4) Lebedev, N.; Trammell, S. A.; Spano, A.; Lukashev, E.; Griva, I.; Schnur, J. Conductive Wiring of Immobilized Photosynthetic Reaction Center to Electrode by Cytochrome c . *J. Am. Chem. Soc.* **2006**, *128*, 12044–12045.
- (5) Das, R.; Kiley, P. J.; Segal, M.; Norville, J.; Yu, a. A.; Wang, L.; Trammell, S. a.; Reddick, L. E.; Kumar, R.; Stellacci, F.; Lebedev, N.; Schnur, J.; Bruce, B. D.; Zhang, S.; Baldo, M. Integration of Photosynthetic Protein Molecular Complexes in Solid-State Electronic Devices. *Nano Lett.* **2004**, *4*, 1079–1083.

- (6) Lebedev, N.; Trammell, S. A.; Tsoi, S.; Spano, A.; Kim, J. H.; Xu, J.; Twigg, M. E.; Schnur, J. M. Increasing Efficiency of Photoelectronic Conversion by Encapsulation of Photosynthetic Reaction Center Proteins in Arrayed Carbon Nanotube Electrode. *Langmuir* **2008**, *24*, 8871–8876.
- (7) Trammell, S. A.; Griva, I.; Spano, A.; Tsoi, S.; Tender, L. M.; Schnur, J.; Lebedev, N. Effects of Distance and Driving Force on Photoinduced Electron Transfer between Photosynthetic Reaction Centers and Gold Electrodes. *J. Phys. Chem. C* **2007**, *111*, 17122–17130.
- (8) Tan, S. C.; Yan, F.; Crouch, L. I.; Robertson, J.; Jones, M. R.; Welland, M. E. Superhydrophobic Carbon Nanotube Electrode Produces a near-Symmetrical Alternating Current from Photosynthetic Protein-Based Photoelectrochemical Cells. *Adv. Funct. Mater.* **2013**, *23*, 5556–5563.
- (9) Sumino, A.; Dewa, T.; Sasaki, N.; Kondo, M.; Nango, M. Electron Conduction and Photocurrent Generation of a Light-Harvesting/Reaction Center Core Complex in Lipid Membrane Environments. *J. Phys. Chem. Lett.* **2013**, *4*, 1087–1092.
- (10) Kondo, M.; Iida, K.; Dewa, T.; Tanaka, H.; Ogawa, T.; Nagashima, S.; Nagashima, K. V. P.; Shimada, K.; Hashimoto, H.; Gardiner, A. T.; Cogdell, R. J.; Nango, M. Photocurrent and Electronic Activities of Oriented-His-Tagged Photosynthetic Light-Harvesting/Reaction Center Core Complexes Assembled onto a Gold Electrode. *Biomacromolecules* **2012**, *13*, 432–438.
- (11) Janssen, P. J. D.; Lambrev, M. D.; Plumeré, N.; Bartolucci, C.; Antonacci, A.; Buonasera, K.; Frese, R. N.; Scognamiglio, V.; Rea, G. Photosynthesis at the Forefront of a Sustainable Life. *Front. Chem.* **2014**, *2*, 36.
- (12) Kothe, T.; Plumeré, N.; Badura, A.; Nowaczyk, M. M.; Guschin, D. A.; Rögner, M.; Schuhmann, W. Combination of a Photosystem 1-Based Photocathode and a Photosystem 2-Based Photoanode to a Z-Scheme Mimic for Biophotovoltaic Applications. *Angew. Chem., Int. Ed.* **2013**, *52*, 14233–14236.
- (13) LeBlanc, G.; Gizzie, E.; Yang, S.; Cliffel, D. E.; Jennings, G. K. Photosystem I Protein Films at Electrode Surfaces for Solar Energy Conversion. *Langmuir* **2014**, *30*, 10990–11001.
- (14) Kargul, J.; Janna Olmos, J. D.; Krupnik, T. Structure and Function of Photosystem I and Its Application in Biomimetic Solar-to-Fuel Systems. *J. Plant Physiol.* **2012**, *169*, 1639–1653.
- (15) Yehezkeili, O.; Tel-Vered, R.; Michaeli, D.; Willner, I.; Nechushtai, R. Photosynthetic Reaction Center-Functionalized Electrodes for Photo-Bioelectrochemical Cells. *Photosynth. Res.* **2014**, *120*, 71–85.
- (16) Kothe, T.; Pöller, S.; Zhao, F.; Fortgang, P.; Rögner, M.; Schuhmann, W.; Plumeré, N. Engineered Electron-Transfer Chain in Photosystem 1 Based Photocathodes Outperforms Electron-Transfer Rates in Natural Photosynthesis. *Chem. – Eur. J.* **2014**, *20*, 11029–11034.
- (17) Ravi, S. K.; Tan, S. C. Progress and Perspectives in Exploiting Photosynthetic Biomolecules for Solar Energy Harnessing. *Energy Environ. Sci.* **2015**, *8*, 2551–2573.
- (18) Sokol, K.; Mersch, D.; Hartmann, V.; Zhang, J. Z.; Nowaczyk, M. M.; Roegner, M.; Ruff, A.; Schuhmann, W.; Plumere, N.; Reiser, E. Rational Wiring of Photosystem II to Hierarchical Indium Tin Oxide Electrodes Using Redox Polymers. *Energy Environ. Sci.* **2016**, *9*, 3698.
- (19) Heering, H. A.; Wiertz, F. G.; Dekker, C.; de Vries, S. Direct Immobilization of Native Yeast Iso-1 Cytochrome C on bare gold: fast electron relay to redox enzymes and zeptomole protein-film voltammetry. *J. Am. Chem. Soc.* **2004**, *126*, 11103–11112.
- (20) De Wael, K.; Bashir, Q.; Van Vlierberghe, S.; Dubruiel, P.; Heering, H. a.; Adriaens, A. Electrochemical Determination of Hydrogen Peroxide with Cytochrome c Peroxidase and Horse Heart Cytochrome c Entrapped in a Gelatin Hydrogel. *Bioelectrochemistry* **2012**, *83*, 15–18.
- (21) Stieger, K. R.; Feifel, S. C.; Lokstein, H.; Lisdat, F. Advanced Unidirectional Photocurrent Generation via Cytochrome c as Reaction Partner for Directed Assembly of Photosystem I. *Phys. Chem. Chem. Phys.* **2014**, *16*, 15667–15674.
- (22) Stieger, K. R.; Feifel, S. C.; Lokstein, H.; Hejazi, M.; Zouni, A.; Lisdat, F. Biohybrid Architectures for Efficient Light-to-Current Conversion Based on Photosystem I within Scalable 3D Mesoporous Electrodes. *J. Mater. Chem. A* **2016**, *4*, 17009–17017.
- (23) Efrati, A.; Tel-Vered, R.; Michaeli, D.; Nechushtai, R.; Willner, I. Cytochrome c-Coupled Photosystem I and Photosystem II (PSI/PSII) Photo-Bioelectrochemical Cells. *Energy Environ. Sci.* **2013**, *6*, 2950.
- (24) Yaghoubi, H.; Lafalce, E.; Jun, D.; Jiang, X.; Beatty, J. T.; Takshi, A. Large Photocurrent Response and External Quantum Efficiency in Biophotocatalytic Cells Incorporating Reaction Center Plus Light Harvesting Complexes. *Biomacromolecules* **2015**, *16*, 1112–1118.
- (25) Friebe, V. M.; Delgado, J. D.; Swainsbury, D. J. K.; Gruber, J. M.; Chanaewa, A.; Van Grondelle, R.; Von Hauff, E.; Millo, D.; Jones, M. R.; Frese, R. N. Plasmon-Enhanced Photocurrent of Photosynthetic Pigment Proteins on Nanoporous Silver. *Adv. Funct. Mater.* **2016**, *26*, 285–292.
- (26) Kamran, M.; Delgado, J. D.; Friebe, V.; Aartsma, T. J.; Frese, R. N. Photosynthetic Protein Complexes as Bio-Photovoltaic Building Blocks Retaining A High Internal Quantum Efficiency. *Biomacromolecules* **2014**, *15*, 2833–2838.
- (27) Dickerson, R. E.; Timkovich, R. Cytochromes c. In *The Enzymes*, 3rd ed.; Boyer, P. D., Ed.; Academic Press: New York, 1975; Vol. 11, pp 397–547.
- (28) Wood, P. M. Why Do c-Type Cytochromes Exist? *FEBS Lett.* **1983**, *164*, 223–226.
- (29) Gerencsér, L.; Laczkó, G.; Maróti, P. Unbinding of Oxidized Cytochrome c from Photosynthetic Reaction Center of *Rhodobacter sphaeroides* Is the Bottleneck of Fast Turnover. *Biochemistry* **1999**, *38*, 16866–16875.
- (30) Schmauder, H.-P.; Pettigrew, G. W.; Moore, G. R. Cytochromes C—Biological Aspects (Springer Series in Molecular Biology, Editor: A. RICH). XIV + 282 S., 68 Abb., 31 Tab. Berlin-Heidelberg-New York-London Paris-Tokyo 1987. Springer-Verlag. DM 198,00. ISBN: 3-540-17843-0. *J. Basic Microbiol.* **1989**, *29*, 191.
- (31) Moser, C. C.; Dutton, P. L. Cytochrome c and c2 Binding Dynamics and Electron Transfer with Photosynthetic Reaction Center Protein and Other Integral Membrane Redox Proteins. *Biochemistry* **1988**, *27*, 2450–2461.
- (32) Friebe, V. M.; Swainsbury, D. J. K.; Fyfe, P. K.; van der Heijden, W.; Jones, M. R.; Frese, R. N. On the Mechanism of Ubiquinone Mediated Photocurrent Generation by a Reaction Center Based Photocathode. *Biochim. Biophys. Acta, Bioenerg.* **2016**, *1857*, 1925–1934.
- (33) Eddowes, M. J.; Hill, H. A. O. Novel Method for the Investigation of the Electrochemistry of Metalloproteins: Cytochrome c. *J. Chem. Soc. Chem. Commun.* **1977**, *0*, 771b.
- (34) Eddowes, M. J.; Hill, H. A. Electrochemistry of Horse Heart Cytochrome c. *J. Am. Chem. Soc.* **1979**, *101*, 4461–4464.
- (35) Song, S.; Clark, R. A.; Bowden, E. F.; Tarlov, M. J. Characterization of Cytochrome C/alkanethiolate Structures Prepared by Self-Assembly on Gold. *J. Phys. Chem.* **1993**, *97*, 6564–6572.
- (36) Millo, D.; Ranieri, A.; Gross, P.; Ly, H. K.; Borsari, M.; Hildebrandt, P.; Wuite, G. J. L.; Gooijer, C.; van der Zwan, G. Electrochemical Response of Cytochrome c Immobilized on Smooth and Roughened Silver and Gold Surfaces Chemically Modified with 11-Mercaptoundecanoic Acid. *J. Phys. Chem. C* **2009**, *113*, 2861–2866.
- (37) Murgida, D.; Hildebrandt, P. The Heterogeneous Electron Transfer of Cytochrome c Adsorbed on Ag Electrodes Coated with ω -Carboxylic Alkanethiols. A Surface Enhanced Resonance Raman Spectroscopic Study. *J. Mol. Struct.* **2001**, *565*, 565–566, 97–100.
- (38) Tarlov, M. J.; Bowden, E. F. Electron-Transfer Reaction of Cytochrome c Adsorbed on Carboxylic Acid Terminated Alkanethiol Monolayer Electrodes. *J. Am. Chem. Soc.* **1991**, *113*, 1847–1849.
- (39) Allen, P. M.; Allen, H.; Hill, O.; Walton, N. J. Surface Modifiers for the Promotion of Direct Electrochemistry of Cytochrome c. *J. Electroanal. Chem. Interfacial Electrochem.* **1984**, *178*, 69–86.

(40) El Kasmi, A.; Wallace, J. M.; Bowden, E. F.; Binet, S. M.; Linderman, R. J. Controlling Interfacial Electron-Transfer Kinetics of Cytochrome c with Mixed Self-Assembled Monolayers. *J. Am. Chem. Soc.* **1998**, *120*, 225–226.

(41) Kato, M.; Zhang, J. Z.; Paul, N.; Reisner, E. Protein Film Photoelectrochemistry of the Water Oxidation Enzyme Photosystem II. *Chem. Soc. Rev.* **2014**, *43*, 6485.

(42) Clark, R. a.; Bowden, E. F. Voltammetric Peak Broadening for Cytochrome c/Alkanethiolate Monolayer Structures: Dispersion of Formal Potentials. *Langmuir* **1997**, *13*, 559–565.

(43) Ke, B.; Chaney, T. H.; Reed, D. W. The Electrostatic Interaction between the Reaction-Center Bacteriochlorophyll Derived from *Rhodospseudomonas spheroides* and Mammalian Cytochrome c and Its Effect on Light-Activated Electron Transport. *Biochim. Biophys. Acta, Bioenerg.* **1970**, *216*, 373–383.

(44) Heering, H. a.; Hirst, J.; Armstrong, F. a. Interpreting the Catalytic Voltammetry of Electroactive Enzymes Adsorbed on Electrodes. *J. Phys. Chem. B* **1998**, *102*, 6889–6902.

(45) Laviron, E. General Expression of the Linear Potential Sweep Voltammogram in the Case of Diffusionless Electrochemical Systems. *J. Electroanal. Chem. Interfacial Electrochem.* **1979**, *101*, 19–28.

(46) Beissenhirtz, M. K.; Scheller, F. W.; Stöcklein, W. F. M.; Kurth, D. G.; Möhwald, H.; Lisdat, F. Electroactive Cytochromec Multilayers within a Polyelectrolyte Assembly. *Angew. Chem., Int. Ed.* **2004**, *43*, 4357–4360.

(47) Swainsbury, D. J.; Friebe, V. M.; Frese, R. N.; Jones, M. R. Evaluation of a Biohybrid Photoelectrochemical Cell Employing the Purple Bacterial Reaction Centre as a Biosensor for Herbicides. *Biosens. Bioelectron.* **2014**, *58*, 172–178.

(48) Collinson, M.; Bowden, E. F.; Tarlov, M. J. Voltammetry of Covalently Immobilized Cytochrome c on Self-Assembled Monolayer Electrodes. *Langmuir* **1992**, *8*, 1247–1250.

(49) Davis, K. L.; Drews, B. J.; Yue, H.; Waldeck, D. H.; Knorr, K.; Clark, R. A. Electron-Transfer Kinetics of Covalently Attached Cytochrome c /SAM/Au Electrode Assemblies. *J. Phys. Chem. C* **2008**, *112*, 6571–6576.

(50) Jeuken, L. J. C. Conformational Reorganisation in Interfacial Protein Electron Transfer. *Biochim. Biophys. Acta, Bioenerg.* **2003**, *1604*, 67–76.

(51) Bowden, E. F. *Interfacial Electrochemistry of Cytochrome c and Myoglobin*; VCU, 1982.

(52) Gupta, R.; Koenig, S.; Redfield, A. On the Electron Transfer between Cytochrome c Molecules as Observed by Nuclear Magnetic Resonance. *J. Magn. Reson.* **1972**, *7*, 66–73.

(53) Millo, D.; Bonifacio, A.; Ranieri, A.; Borsari, M.; Gooijer, C.; Van Der Zwan, G. Voltammetric and Surface-Enhanced Resonance Raman Spectroscopic Characterization of Cytochrome c Adsorbed on a 4-Mercaptopyridine Monolayer on Silver Electrodes. *Langmuir* **2007**, *23*, 4340–4345.

(54) Straley, S. C.; Parson, W. W.; Mauzerall, D. C.; Clayton, R. K. Pigment Content and Molar Extinction Coefficients of Photochemical Reaction Centers from *Rhodospseudomonas spheroides*. *Biochim. Biophys. Acta, Bioenerg.* **1973**, *305*, 597–609.